nature chemical biology

ARTICLE

PUBLISHED ONLINE: 28 SEPTEMBER 2014 | DOI: 10.1038/NCHEMBIO.1639

Unraveling the mechanism of cell death induced by chemical fibrils

Olivier Julien[1], Martin Kampmann[2,3], Michael C Bassik[2,9], Julie A Zorn[1,9], Vincent J Venditto[4], Kazutaka Shimbo[1,9], Nicholas J Agard[1,9], Kenichi Shimada[5], Arnold L Rheingold[8], Brent R Stockwell[5–7], Jonathan S Weissman[2,3] & James A Wells[1,2]*

We previously discovered a small-molecule inducer of cell death, named 1541, that noncovalently self-assembles into chemical fibrils ('chemi-fibrils') and activates procaspase-3 *in vitro*. We report here that 1541-induced cell death is caused by the fibrillar rather than the soluble form of the drug. A short hairpin RNA screen reveals that knockdown of genes involved in endocytosis, vesicle trafficking and lysosomal acidification causes partial 1541 resistance. We confirm the role of these pathways using pharmacological inhibitors. Microscopy shows that the fluorescent chemi-fibrils accumulate in punctae inside cells that partially colocalize with lysosomes. Notably, the chemi-fibrils bind and induce liposome leakage *in vitro*, suggesting they may do the same in cells. The chemi-fibrils induce extensive proteolysis including caspase substrates, yet modulatory profiling reveals that chemi-fibrils form a distinct class from existing inducers of cell death. The chemi-fibrils share similarities with proteinaceous fibrils and may provide insight into their mechanism of cellular toxicity.

Many neurodegenerative diseases are associated with the accumulation of protein fibrils in the brain. These include amyloid-β in Alzheimer's disease, superoxide dismutase-1 (SOD1) in amyotrophic lateral sclerosis, prion protein in Creutzfeldt-Jakob disease and α-synuclein in Parkinson's disease[1]. In these disorders, the accumulation of abnormally folded proteins, rich in β-sheets, results in the formation of aggregates that can lead to cytotoxicity. Numerous studies have revealed many important features of these protein misfolding diseases both at the structural and biological levels[2]. However, the precise cellular mechanisms by which extracellular protein aggregates lead to cellular toxicity remain unresolved.

A high-throughput screen performed in our laboratory identified a small molecule, called 1541 (**Fig. 1a**), that activates the executioner procaspase-3 *in vitro*[3]. The compound induces caspase activation and cell death in various cancer cell lines as quickly as the most potent apoptotic inducers known. Compound 1541 (molecular weight = 411 Da) and its derivatives induce caspase-3 activation and cell death through a mechanism that is not wholly dependent upon the well-studied intrinsic (caspase-9) or extrinsic (caspase-8) pathways[3]. To our surprise, we found that 1541 and other active analogs rapidly self-assemble in aqueous solution into chemical fibrils[4] (**Fig. 1b**); we call them chemi-fibrils to distinguish them from natural proteinaceous fibrils. We showed that procaspase-3 localizes and becomes activated on the chemi-fibrils or proteinaceous amyloid-β fibrils *in vitro*[5]. Compared to proteinaceous fibrils, 1541 and analogs are remarkably simple to synthesize and form fibrils immediately upon addition to aqueous solution, making them much easier to handle and to study *in vitro* and in cells.

Here, using various biochemical and biophysical methods, we show that the chemi-fibrils, not the free soluble small molecule, induce cell death in mammalian culture. We used diverse methods including short hairpin RNA (shRNA) screens[6–8], chemical genetic approaches[9], N-terminomics (to identify protease involvement)[10–12], modulatory profiling (to help classify the cellular mechanism of chemi-fibrils)[13] and cell biology tools to show how chemi-fibrils enter cells and induce cell death. Remarkably, the chemi-fibrils enter through the endocytic pathway and traffic to lysosomes, leading to activation of intracellular proteases, including caspases. We believe that these synthetic chemi-fibrils may provide valuable insights into how extracellular fibrillar structures can induce cell death.

RESULTS

Structural characterization of 1541

Individual molecules of compound 1541 rapidly self-assemble into well-ordered nanofibrils, as observed by EM[4] (**Fig. 1b**). We wished to understand the intermolecular packing of 1541 because, unlike protein-forming fibrils, 1541 presents very little opportunity for hydrogen bonding. We determined the X-ray structure of 1541 at atomic resolution to reveal the intermolecular interactions between the small molecules (**Fig. 1c**; crystal data and structure refinement can be found in **Supplementary Results**, **Supplementary Fig. 1**). The small molecules are strictly planar and stack on each other with a separation of 0.34 nm. However, each small molecule is shifted by 0.64 nm so that there is no perpendicular ring stacking. Considering that each 1541 molecule is 1.5 nm wide and that each individual fibril is as thin as 2.6 nm, as observed by transmission EM (TEM), it is conceivable that the fibrils may be only two or three 1541 molecules in width. Fiber diffraction studies will be needed to confirm that this packing arrangement is preserved in the chemi-fibrils as well as to define the fiber axis. Nonetheless, these data show that tight packing can be achieved in these chemi-fibrils, forming

[1]Department of Pharmaceutical Chemistry, University of California–San Francisco, San Francisco, California, USA. [2]Department of Cellular and Molecular Pharmacology, University of California–San Francisco, San Francisco, California, USA. [3]Howard Hughes Medical Institute, University of California–San Francisco, San Francisco, California, USA. [4]Department of Bioengineering and Therapeutic Sciences, University of California–San Francisco, San Francisco, California, USA. [5]Department of Biological Sciences, Columbia University, New York, New York, USA. [6]Department of Chemistry, Columbia University, New York, New York, USA. [7]Howard Hughes Medical Institute, Columbia University, New York, New York, USA. [8]Department of Chemistry, University of California–San Diego, San Diego, California, USA. [9]Present addresses: Department of Genetics, Stanford University School of Medicine, Stanford, California, USA (M.C.B.); Department of Molecular and Cell Biology, University of California–Berkeley, Berkeley, California, USA (J.A.Z.); Ajinomoto Co., Inc., Japan (K.S.); Codexis Inc., Redwood City, California, USA (N.J.A.). *e-mail: jim.wells@ucsf.edu

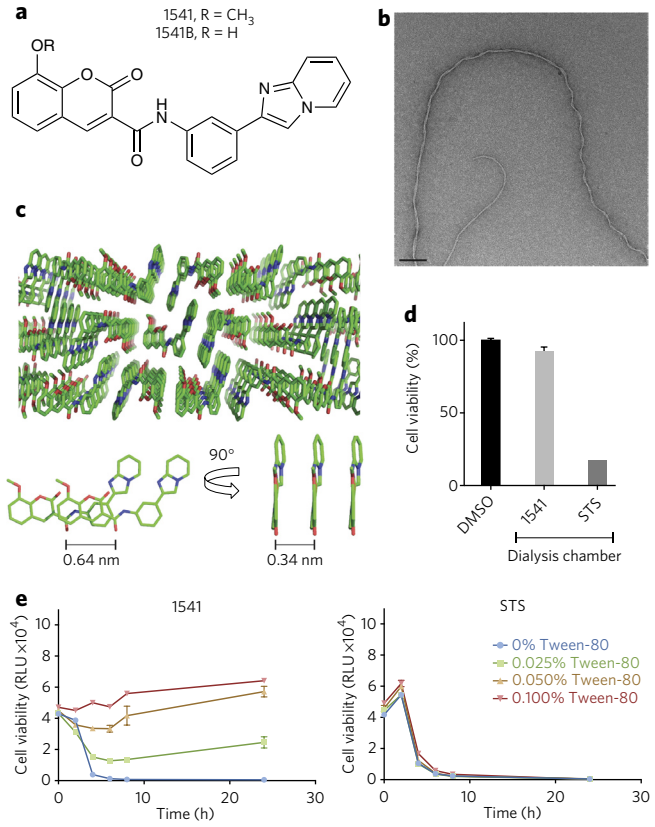

Figure 1 | 1541 forms chemi-fibrils that induce cell death in cell culture. (**a**) Chemical structure of 1541 (R = CH_3) and its analog 1541B (R = OH). (**b**) Transmission electron micrograph of the chemical fibrils. Scale bar, 100 nm. (**c**) Crystal structure of 1541 showing the small-molecule stacking from three different views. (**d**) Chemi-fibrils induce cell death, but the monomers do not. 1541 or STS was added into a dialysis chamber that was placed into a dish of K562 cells. Cell viability after 48 h was measured. (**e**) The nonionic detergent Tween-80 disrupts 1541 cell death activity but has no effect on STS. Cell viability was monitored using CellTiter-Glo (RLU, raw luminescence unit). The data represent mean values ±s.d. (n = 3).

molecules without intricate hydrogen bonding networks typical of proteinaceous fibrils[14].

Cell death is induced by the chemi-fibrils not monomers

We have previously shown by TEM and dynamic light scattering (DLS) that the chemi-fibrils of 1541 form within the mixing time when added from DMSO to neutral buffers. The chemi-fibrils also form immediately when transferred from DMSO to cell culture medium (**Supplementary Fig. 2**). Notably, the threshold concentration required for formation of 1541 chemi-fibrils in cell culture (~2 μM), as observed by DLS, matches the approximate half-maximum effective concentration (EC_{50}) required for cell death induced by mammalian cells[3]. We have shown that the chemi-fibrils are apparently kinetically trapped once they are formed. For example, when a dialysis chamber was placed in a buffer containing 1541 chemi-fibrils, we could not detect 1541 inside the chamber over a 12-h period at 37 °C (**Supplementary Fig. 3**). Furthermore, 1541 will not activate procaspase-3 *in vitro* when the two are separated by a dialysis membrane[4]. We conducted an analogous experiment to determine whether 1541 can induce cell death when partitioned by a dialysis membrane, using the immortalized myelogenous leukemia line K562, which is commonly used in cell death studies. Also, K562 cells conveniently grow readily in suspension and perform well in pooled shRNA screens[7]. As with other cell lines we have tested, K562 cells are highly sensitive to 1541-induced cell death, as shown by a drop in ATP levels and caspase activation (**Supplementary Fig. 4**). However, when K562 cells were exposed to 1541 sequestered in a dialysis bag (molecular weight cutoff of 3.5 kDa), the cells did not undergo cell death over a 48-h period (**Fig. 1d** and **Supplementary Fig. 5**). In contrast, staurosporine (STS; molecular weight = 466 Da), a promiscuous protein kinase inhibitor that induces apoptosis in a variety of cell types and does not form aggregates, causes rapid cell death when cells are exposed directly or isolated behind the dialysis membrane. The same results occurred when cells were placed inside the dialysis bag and the small molecules were placed outside (**Supplementary Fig. 6**).

One way to perturb small-molecule aggregators is to use small amounts of nonionic detergent in cell culture[15]. Specifically, Tween-80 is able to dissolve small-molecule aggregators and has negligible toxicity in cell culture when dosed less than 0.1% (**Supplementary Fig. 7**)[15]. We found that Tween-80 protects cells in a dose-dependent manner from 1541-induced cell death (**Fig. 1e**) but does not protect cells from killing by STS (**Fig. 1e**). Tween-80 does not perturb the cellular uptake of 100-nm-wide fluorescent nanoparticles[16], so these effects are unlikely to be caused by blocking endocytosis. In addition, we found that centrifugation of the 1541-containing cell culture medium led to a toxic pellet and a nontoxic supernatant (**Supplementary Fig. 8**). Overall, all of our results indicate that 1541 chemi-fibrils, not the 1541 monomer, induce cell death.

shRNA screen reveals genes important for fibril toxicity

To probe how the chemi-fibrils induce cell death in cell culture, we performed a functional genomic screen using ultracomplex short-hairpin RNA (shRNA) libraries (**Fig. 2a**). We sought to identify genes that, when knocked down, would protect or sensitize cells against chemi-fibril–induced apoptosis. K562 cells were transduced using lentiviral shRNA libraries. The sublibraries we used together target more than 4,000 genes with 25 shRNAs each and include more than 500 negative control shRNAs per sublibrary[7]. Cells were stimulated with compound 1541 (treated) or DMSO (untreated) for four or five cycles over 20 d (**Supplementary Fig. 9**). The cellular DNA was then extracted from the two populations, and the shRNA-encoding cassette was amplified by PCR. The frequencies of cells expressing each shRNA were quantified in both populations by deep sequencing, and quantitative phenotypes were derived using previously described methodology[8,17]. After averaging shRNA phenotypes from two replicate screens, genes with statistically significant protective and sensitizing phenotypes were identified by comparing the phenotypes of shRNAs targeting a given gene to the phenotypes of the negative control shRNAs using P values based on the Mann-Whitney U test. We found several strong hit genes, such as *RAB1A* (**Supplementary Fig. 10**), for which the vast majority of 25 shRNAs that targeted them protected cells from 1541 toxicity. The top hits are labeled in **Figure 2b**, showing the good reproducibility between experimental replicates. The full list of genes for the two replicate screens and their P values are presented in **Supplementary Data Set 1**. Notably, we identified several strong hits for genes encoding proteins involved in endocytosis and vesicle trafficking. More specifically, the shRNA screen analysis revealed a major role for the Rab GTPase family in chemi-fibril–induced cell death, including members RAB1A, RAB2A, RAB39A, RAB7A as well as RABEP1 (**Supplementary Data Set 1**). These small proteins have a substantial role in vesicle trafficking: RAB1A and RAB2A are particularly important for ER-Golgi transport[18], RAB7A has been involved in vesicle trafficking from late endosomes to lysosomes[19], and RABEP1 is involved in early endosome fusion[20], whereas RAB39A has recently been linked to phagosome acidification[21] (see ref. 22 for a review). Moreover, we found that V-ATPase, a protein complex essential for acidification of intracellular organelles including lysosomes, also has a notable role in cell death induced by chemi-fibrils.

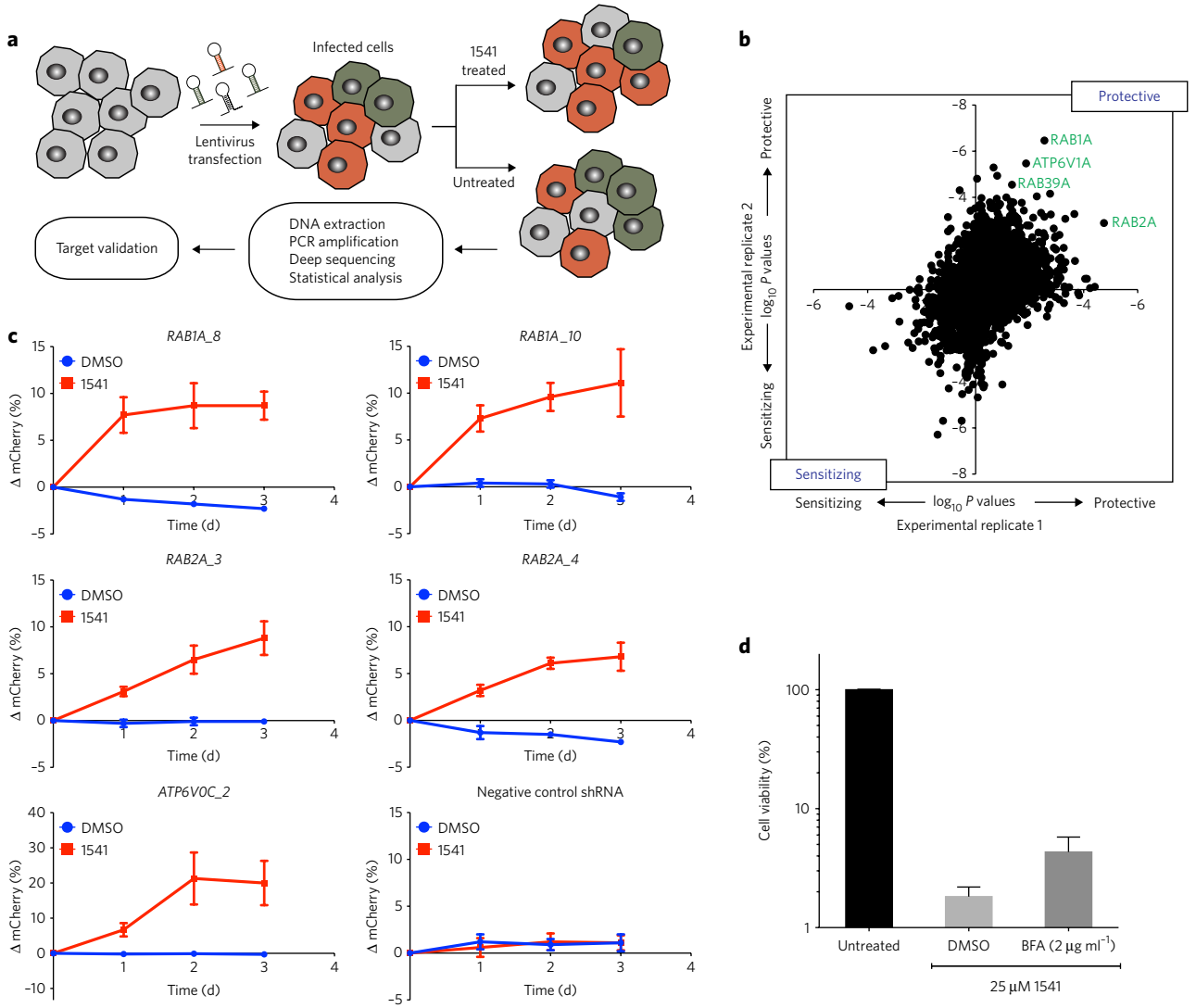

Figure 2 | shRNA screen reveals a major role of vesicle trafficking and lysosome acidification in 1541 chemi-fibril–induced cell death. (**a**) Experimental strategy to screen for protective and sensitizing genes against chemi-fibrils. The shRNA screen was performed in two independent replicates. (**b**) Protective and sensitizing genes (~4,000 tested genes) as determined by two-sided Mann-Whitney *U* test score. Some of the strongest hits are members of the Rab family of GTPases, regulating steps of vesicle formation and trafficking. (**c**) Protective effect of knocking down *RAB1A*, *RAB2A* and *ATP6V0C* genes. Starting with a 50:50 population of wild-type and transfected cells, the population of cells expressing a shRNA (and mCherry) targeting a gene of interest showed protection against 1541 after 24–72 h of treatment, as monitored by flow cytometry. The error bars represent mean change ±s.e.m. for five independent experiments. (**d**) Cell viability assay quantifying the protection effect of brefeldin A (BefA) against chemi-fibril–induced cell death after 6 h. HeLa cells were treated with BefA for 30 min and then treated with 25 μM 1541. Cell viability was assessed using CellTiter-Glo, and the reported values correspond to mean values ±s.d. (n = 3). See **Supplementary Figure 8** for full dose response of BefA as a function of time, including DMSO and STS controls.

Among the top protective hits (based on their *P* value) were genes encoding RAB1A, RAB2A and a member of the V-ATPase complex. To validate the screening results, we created stable knockdown cell lines expressing single shRNA targeting the genes *RAB1A*, *RAB2A* or *ATP6V0C* (**Fig. 2c**). In these cell lines, the targeted genes were depleted by more than 60%, as assessed by real-time PCR (**Supplementary Fig. 11**). To validate the protective effect of these genes, we mixed equal amounts of wild-type K562 cells and K562 cells expressing a given shRNA (and mCherry) and monitored the phenotype caused by the shRNA as the change in the percentage of mCherry-positive cells in the population, as quantified by flow cytometry. As expected, the fraction of cells expressing a protective shRNA targeting *RAB1A* or *RAB2A* showed a marked increase (percentage) over the wild-type population after chemi-fibril treatment (**Fig. 2c**), whereas the population of cells expressing a control shRNA did not show any change. Consistent with these results, we found that the pretreatment of HeLa cells with brefeldin A, an inhibitor of vesicular transport between the ER and the Golgi apparatus, delayed cell death induced by chemi-fibrils (**Fig. 2d**) but not by STS (**Supplementary Fig. 12**). To mimic the knockdown of V-ATPase, we found that chloroquine, a lysosomotropic agent, and bafilomycin, an endosomal acidification inhibitor, also weakly protected against 1541 cell death (**Supplementary Fig. 13**). Together, the shRNA knockdown and pharmacological inhibitor studies suggest that intracellular vesicle trafficking and lysosome acidification are important for chemi-fibril–induced cell death.

Chemi-fibrils enter cells and traffic to lysosomes

The presence of the coumarin ring in 1541 makes it conveniently fluorescent for microscopy studies (**Supplementary Fig. 14**).

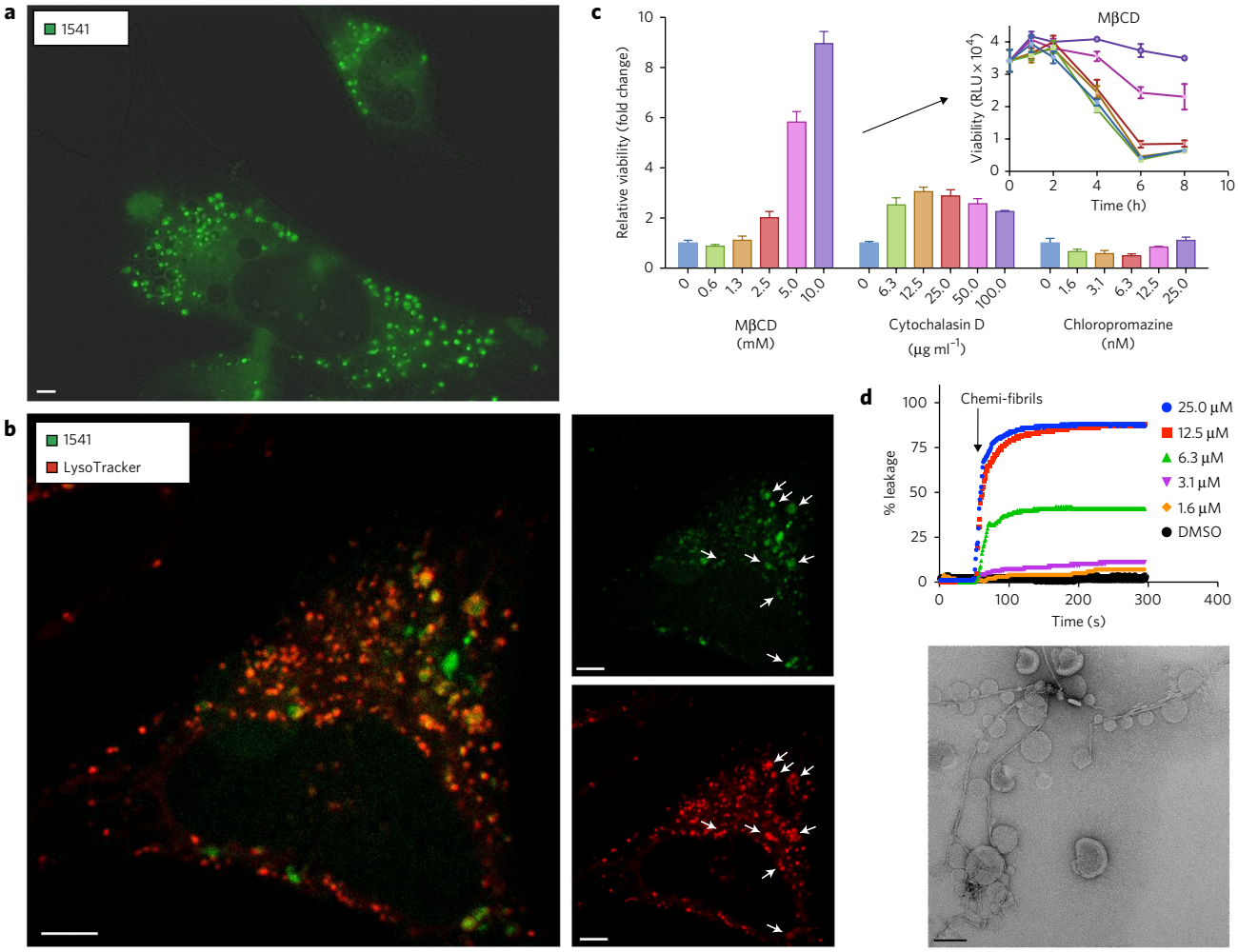

Figure 3 | Internalization of fluorescent aggregates in cell and specific endocytosis inhibition delay cell death. The presence of a fluorescent coumarin ring in the chemical structure of 1541 (**Fig. 1a**) is a convenient way to track chemi-fibrils in live cells. (**a**) HeLa cells were treated with 1541, and live cell imaging (DAPI channel, shown in green) was used to monitor the accumulation of chemi-fibrils into punctae inside a cell. (**b**) LysoTracker images show partial colocalization to acidic vesicles. In **a** and **b**, scale bars are 5 μm. (**c**) Inhibition of endocytosis can partially protect against chemi-fibril–induced cell death after 6 h of treatment with 20 μM of 1541. MβCD and cytochalasin D delayed cell death, whereas chloropromazine did not. Cell viability was assessed using CellTiter-Glo in triplicate experiments, and the reported protection values correspond to raw luminescence units (RLU; data represent mean values ±s.d.) normalized on cells treated with only 1541 (no inhibitors). (**d**) Top, chemi-fibrils induce liposome leakage *in vitro*. Bottom, EM image shows the clear interaction between the chemi-fibrils and liposomes. Scale bar, 100 nm. Data are representative of two independent experiments.

We exploited the fluorescence of 1541 to examine the uptake of chemi-fibrils and their intracellular trafficking. To facilitate analysis by fluorescence microscopy, we used HeLa cells, which are adherent and have a similar sensitivity to 1541-induced cell death as K562 cells[15]. Prior to cell death, large fluorescent punctae formed within hours of treatment of HeLa cells with 1541 (**Fig. 3a**). We attribute these fluorescent punctae to 1541 as they were not observed in cells treated with other nonfluorescent cell-death inducers such as FasL (**Supplementary Fig. 15**). To determine the localization of these punctae, we used organelle markers such as ER-Tracker, MitoTracker and LysoTracker. The fluorescent punctae partially localized with LysoTracker (**Fig. 3b**), suggesting some localization to lysosomes, endosomes or both and not with the ER or the mitochondria (**Supplementary Figs. 16** and **17**). We further confirmed the colocalization of fluorescent punctae with lysosomes using HeLa expressing LAMP1-GFP (**Supplementary Fig. 18**). It is possible that some of the few fluorescent punctae that do not overlap with known organelle markers are present in nonlysosomal vesicles or correspond to the accumulation of cytosolic chemi-fibrils. Overall, these images support that chemi-fibrils are able to enter mammalian cells, most likely via endocytosis, before inducing cell death.

Inhibitors of endocytosis partially protect against death

To validate the importance of endocytosis in the 1541 cell death mechanism using an orthogonal approach, we tested specific endocytosis inhibitors (cytochalasin D, methyl-β-cyclodextrin (MβCD) and chloropromazine) that have previously been used to study the uptake of amyotrophic lateral sclerosis–causing SOD1 mutant aggregates[23]. We discovered that inhibition of certain endocytic pathways could protect cells against chemi-fibril-induced cell death (**Fig. 3c**). Specifically, MβCD, which disrupts lipid rafts by removing cholesterol from membranes, showed the strongest protective effect. The MβCD was shown by DLS not to disrupt chemi-fibril formation (**Supplementary Fig. 19**), a distinct possibility as it is known to bind hydrophobic molecules such as 1541. The fact that MβCD is not disruptive to 1541 chemi-fibrils is consistent with the very slow dissociation of monomers from the

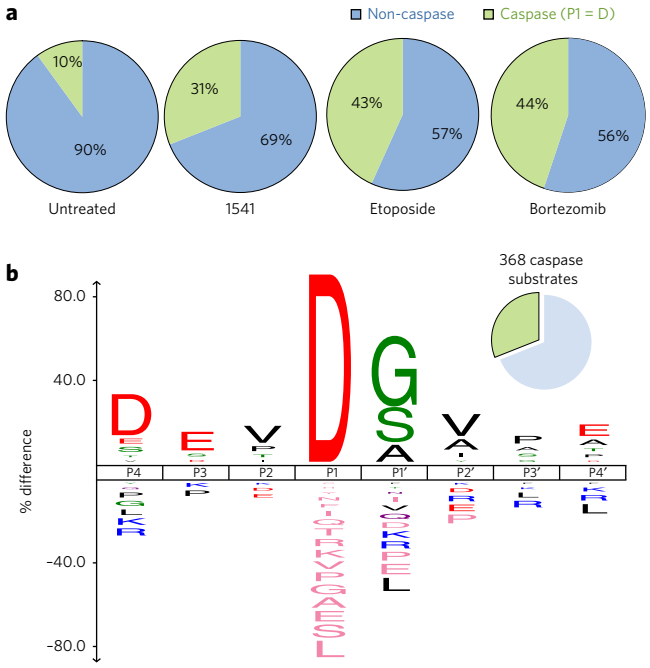

Figure 4 | Cell death induced by chemi-fibrils induces proteolysis with prominent caspase cleavages. (**a**) Using our N-terminal labeling technology[12], we found 703 peptides containing an aspartic acid at the P1 position (out of 2,980 peptides), corresponding to 368 substrates (31% of the total) having caspase-like cleavage sites plus 819 substrates cleaved by other unidentified proteases. These results were obtained using two independent experiments: one treating HeLa cells with 1541 and one adding 1541B to DB lymphoma cells. In comparison, only 10% of the total protein substrates can be observed in untreated cells[10]. (**b**) Consensus sequence from P4-P4′ for the caspase cleavage sites identified during cell death induced by chemi-fibrils. The figure shows the dominance of a DEVD consensus sequence, supporting the activation of executioner caspases during apoptosis.

chemi-fibrils. Cytochalasin D, which inhibits actin polymerization, had a small protective effect, and chloropromazine, which disrupts clathrin-dependent endocytosis, had no effect. We did not observe colocalization of 1541 chemi-fibrils with HIV TAT-TAMRA peptides, common markers of macropinocytosis that colocalize with SOD1 and tau aggregates[14] (**Supplementary Fig. 20**). These results suggest that chemi-fibrils enter cells using endocytosis to induce cell death.

Chemi-fibrils lead to liposome leakage

Given that chemi-fibrils can directly enter the endocytic pathway, we asked whether or how these fibrils may escape vesicles. The release of encapsulated self-quenching carboxyfluorescein from liposomes is commonly used to test the integrity of lipid bilayers[24]. Various concentrations of 1541 chemi-fibrils were added to carboxyfluorescein-containing liposomes. The addition of chemi-fibrils rapidly caused a large fluorescence increase in a dose-dependent manner (**Fig. 3d**) that matched the threshold concentration for fibril formation as monitored by DLS as well as the EC_{50} for cell death. Moreover, the chemi-fibrils directly bind liposomes, as evidenced by TEM (**Fig. 3d**). These results indicate that chemi-fibrils are capable of binding lipid vesicles and inducing leakage. Thus, the chemi-fibrils may escape from or cause leakage of endocytic vesicles or downstream compartments such as lysosomes.

Given the broad activity and unique mechanism for cell death by 1541, we wondered whether 1541 would be cytotoxic to microbes as well. Many antibacterials kill by puncturing membranes, and 1541 could potentially behave similarly. However, we found that 1541 had no impact on growth or survival of yeast, *Escherichia coli* or *Bacillus subtilis* (**Supplementary Fig. 21**).

Chemi-fibrils induce widespread proteolysis

Previous studies have shown that 1541-mediated cell death is independent of both typical intrinsic and extrinsic apoptotic pathways yet does activate caspases[3]. We investigated the extent to which 1541 induced proteolysis using N-terminomics, a method our laboratory developed for identifying the products of intracellular proteases through enzymatic tagging of newly generated N termini[11]. Using the N-terminomics technology, we determined that cell death induced by chemi-fibrils generates many proteolytic cleavage sites typical of executioner caspases. Nearly 31% (703 of 2,980 peptides, 368 of 1,187 proteins) of the substrates identified from 1541-treated cells resulted from cleavage after aspartic acid, a hallmark of caspase cleavages (**Fig. 4a**). These results were generated across two cell lines, HeLa S3 and DB lymphoma cells, and many of the cleaved substrates were shared by other apoptotic inducers, such as etoposide and bortezomib[11,25,26] (http://wellslab.ucsf.edu/degrabase/)[10]. Only 10% of these protein substrates were observed in untreated cells, which probably represent a typical small population of dying cells in the cell culture. More than 70% of the substrates found in the chemi-fibril data set are identical to those found in cells treated with bortezomib, a stronger inducer of intrinsic apoptosis (**Supplementary Data Set 2**). Furthermore, the consensus sequence from P4-P4′ for the caspase cleavage sites identified during cell death induced by chemi-fibrils shows the presence of the hallmark DEVD consensus sequence (**Fig. 4b**), consistent with the activation of executioner caspases. There are many other noncaspase substrates that are generated, suggesting the potential activation of other proteases, too. In addition to the activation of caspases and their substrates, we observed important membrane blebbing in HeLa cells upon 1541 treatment using live cell imaging (**Supplementary Videos 1** and **2**), which is one of the hallmarks of apoptosis. We also observed the formation of very large clumps of cells only a few hours after adding chemi-fibrils to suspension cells (**Supplementary Fig. 22**).

Modulatory profiling suggests an atypical death mechanism

To further compare chemi-fibril–induced cell death to other known cell death inducers, we profiled small molecules for their ability to modulate the lethality of 1541 using a previously described method[13]. In short, the changes in the lethality of chemi-fibrils when used in combination with each member of a panel of cell death modulators are reported. Model-based clustering[27] identified eight distinct clusters and the membership of 71 lethal profiles in these clusters (**Fig. 5a**). Compound 1541 and its analog (1541B) formed a unique cluster in this analysis. The modulatability scores for 1541 were as low as compounds with reactive moieties or hydrophobic amines (**Fig. 5b**). However, because 1541 and its analog do not contain hydrophobic amines or reactive moieties, and because we found that the lethality of 1541 and its analog could be suppressed by specific shRNAs and vesicle trafficking inhibitors, we conclude that these compounds induce cell death through a distinct mechanism. Notably, the pan-caspase inhibitor, z-VAD-fmk, provided only mild protection from 1541-induced cell death (1.7-fold increase in protection; **Fig. 5c**), suggesting that 1541 can also induce caspase-independent cell death. From the modulatory profiling experiments, it seems that chemi-fibrils belong to a new cluster of cell death inducers distinct from those covered by the original modulatory profiles described in ref. 13. This noncovered cluster could potentially include other untested fibrillar structures, such as amyloid-β or crystalline substances such as cholesterol crystals and sodium urate, which are capable of inducing an inflammatory response[28,29].

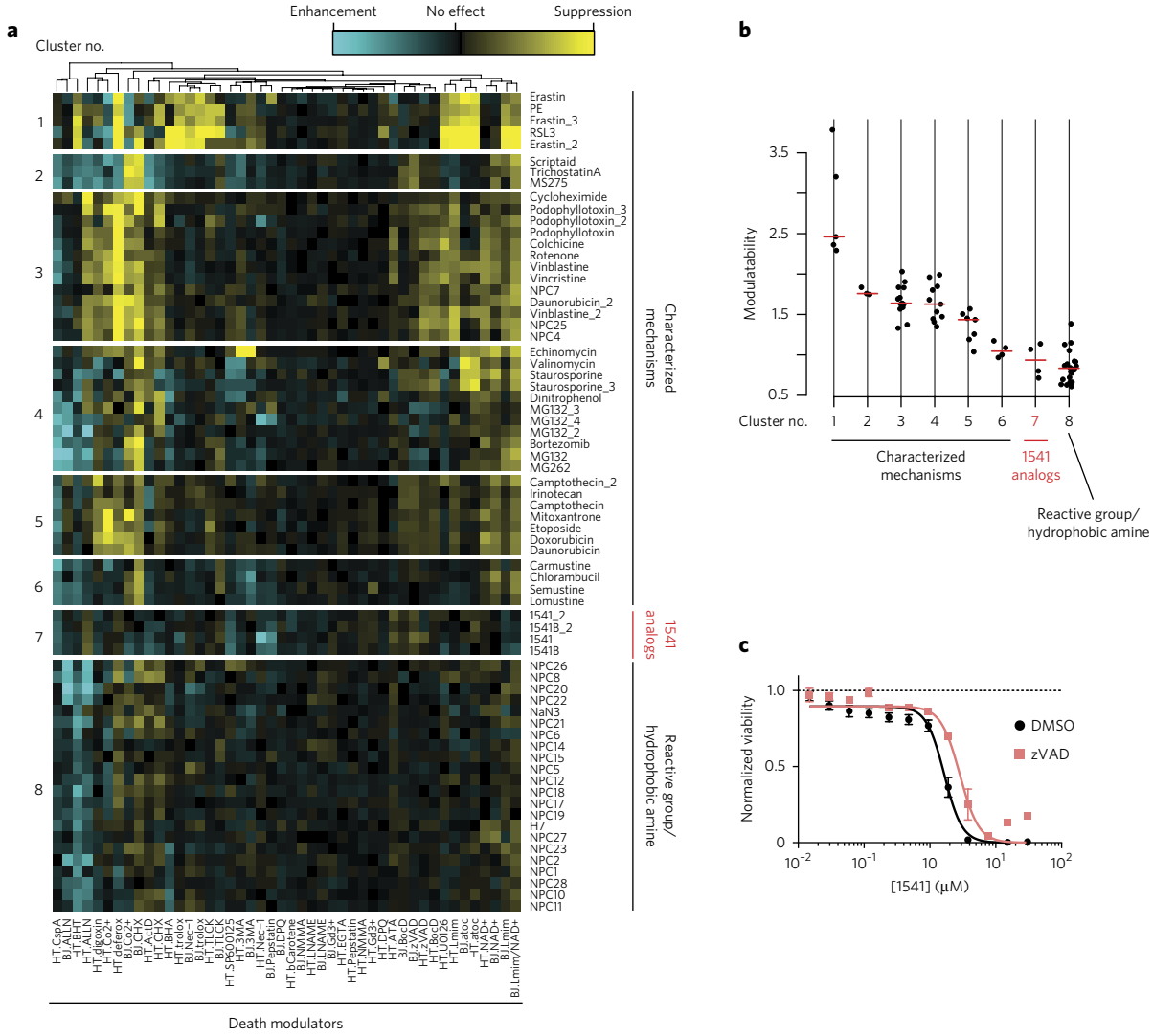

Figure 5 | Modulatory profiling suggests 1541 and an analog form a unique class of compounds that induce cell death only partially delayed by blocking caspases. The changes in the lethality of chemi-fibrils when used in combination with each member of a panel of cell death modulators are presented. (**a**) Lethal compounds are clustered based on their 'modulatability', the extent to which their effect is modulated by other molecules. Modulatability values are represented by heat map colors. Model-based clustering identified eight distinct clusters among 1541 analogs and other characterized lethal compounds. The profiles of all 1541 analogs formed a unique cluster, which suggest that their mechanism of cell death is distinct from that of the other tested compounds. They have a low modulatability overall (i.e., the lethality did not change very much with chemical modulators). (**b**) Modulatability scores of compounds in eight clusters. Cluster number is the same as in **a**. The red bar indicates the median modulatability score of each cluster. The modulatability of 1541 analogs is as small as that of reactive or hydrophobic amines, although their physicochemical properties are distinct from those of 1541 analogs. (**c**) Representative dose-curve showing that 1541 analogs are mildly suppressed by pan-caspase inhibitors. The shift in EC_{50} values for 1541 lethality upon zVAD treatment was 1.7-fold, which was significantly deviated from zero with a probability of 1.5×10^{-5} (extra sum-of-squares F test). The data represent mean values ±s.e.m. ($n = 3$).

DISCUSSION

Using a combination of technologies, we have further elucidated the cellular mechanism of 1541-induced cell death and present a working hypothesis that summarizes our data (**Fig. 6**). We find that 1541 chemi-fibrils form instantaneously in water, buffer solutions or cell culture medium. Dialysis, Tween-80 and MβCD protection studies strongly suggest the fibrils, and not the monomer, enter the cell and are responsible for cell killing. In fact, 1541 fibril formation, liposome leakage and cell death all occur in the same concentration range, starting at ~2–3 μM. Several lines of evidence suggest that the chemi-fibrils enter cells through endocytosis. For example, inhibitors of endocytosis such as brefeldin A and MβCD restrict 1541-induced cell death without interfering with fibril formation. We saw fluorescent punctae in cells that we attribute to intracellular accumulation of the fluorescent chemi-fibrils, which precedes cell death. We did not observe obvious cell breakage in cell culture, but we did observe membrane blebbing, which is typical of apoptosis.

Our fluorescence data suggest that the vesicles containing the chemi-fibrils partly colocalize to lysosomes but not to mitochondria or the ER. The shRNA screen identified several genes that, when knocked down, provided some protection from cell death, including several Rab GTPases important in vesicle trafficking and V-ATPase, an important lysosomal proton pump. We have shown that chemi-fibrils bind liposomes and induce leakage *in vitro*, suggesting that the fibrils might be able to escape intracellular vesicles. One possibility is that chemi-fibrils traffic to lysosomes, induce their breakage and leak their contents. The caspases, among other proteases, ultimately become activated, and more than 85% of the detected cleaved products

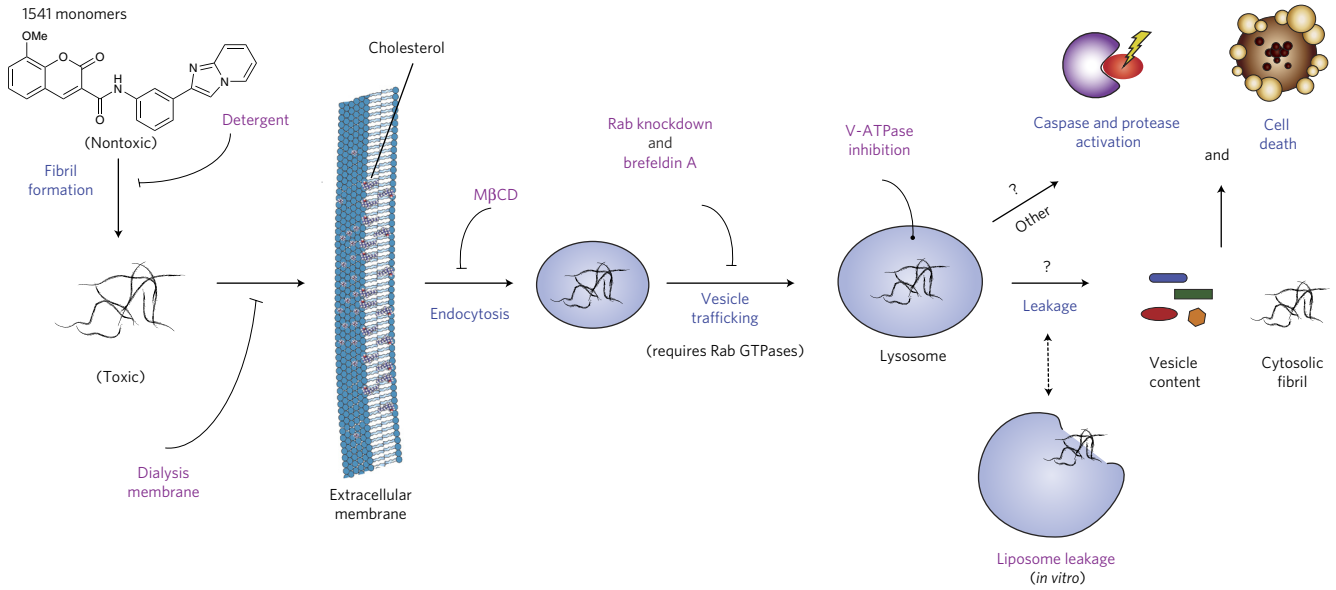

Figure 6 | Proposed mechanism of cell death induced by 1541 chemi-fibrils. The small molecules form fibrils in cell culture medium. Dialysis or nonionic detergents can block the cellular entry of chemi-fibrils. Otherwise, the chemi-fibrils enter the cells, as shown by fluorescence microscopy, using endocytic mechanisms, which can be partially blocked by MβCD and brefeldin A. The chemi-fibrils most likely traffic within the cells, as shown by shRNA protection experiments, and can localize to lysosomes. They can cause vesicles to leak their content, which could allow the chemi-fibril and/or the vesicle content to reach the cytosol, resulting in activation of the caspases and possibly other proteases. The chemi-fibrils can induce a mixed form of cell death, unique from that of other compounds profiled, that shares some hallmarks of apoptosis, such as membrane blebbing.

are also observed for other apoptotic inducers (**Supplementary Data Set 2**). On the basis of the sequence logo of the substrates with non–aspartic acid at P1, some of these unidentified proteases could be cathepsins, trypsin-like proteases or calpains. The major obstacle in confirming these important proteases is distinguishing meaningful cleavages over background (i.e., untreated cells). Yet, the precise mechanism of cell death appears distinct from that of other known cell death–inducing small molecules, as shown by comparisons with other toxic compounds using modulatory profiling[13]. However, much like crystalline substances capable of inducing an inflammatory response in macrophages, such as cholesterol and sodium urate crystals[28,29], the chemi-fibrils involve uptake to lysosomes and induce caspase activation that leads to cell death. The chemi-fibrils are more potent than these inflammatory stimuli and induce cell death in mammalian cell lines[3] that are not known to activate the NLRP3 inflammasome pathway. Pan-caspase inhibitors were only mildly protective, and caspases were not strong hits in the shRNA screen. In fact, the protective effects we observed in the shRNA screen were partial, suggesting that none of the 4,000 target genes are able to completely protect from 1541 cell death. Our data suggest that there may be parallel cell death mechanisms at work, involving both caspase-dependent and caspase-independent mechanisms. For example, two uncharacterized GPCRs (GPR171 and GPR174) have been identified as protective hits (**Supplementary Data Set 1**). It is possible that an alternate mechanism involving extracellular receptors such as GPCRs could have a role here in regulating endocytosis or initiating signal transduction.

There are intriguing parallels and differences between these synthetic chemi-fibrils and natural protein amyloid fibrils[30], which also form micron-long fibrillar structures. The X-ray structure of crystalline 1541 suggests a tight and dry intermolecular packing of the small molecules, which is much like the steric zipper structures of short protein segments that form fibrils from SOD1, tau and amyloid-β (ref. 2). However, intermolecular 1541 interactions lack any of the characteristic hydrogen bonding interactions prominent in the β-sheet structures. It has been shown that amyloid fibrils of mammalian prion proteins are toxic to cultured cells and primary neurons[31] and that adding them to cell culture leads to cell aggregation and the formation of cell clumps. Similarly, we observed formation of very large clumps of cells only a few hours after adding chemi-fibrils to K562 cells. Also, the same small molecules that slow the uptake of fluorescently labeled SOD1 aggregates by human cells[23] also protect against chemi-fibrils, suggesting analogous uptake mechanisms. The compound that provided the greatest protection from 1541-induced cell death was MβCD, which has been recently shown to have a protective effect in neuronal cell culture and in a transgenic mouse model of Alzheimer's disease[32]. Notably, both 1541 fibrils and Aβ-fibrils can activate procaspase-3 *in vitro*[4]. Compelling evidence in the neurodegenerative disease field also suggest that small protein oligomers have a major role in neurotoxicity[33]. This might be the case for chemi-fibrils as well, but more studies will be required to address this complex subject.

Chemi-fibrils may prove to be useful tools to better understand the mechanism of extracellular neurotoxic fibrils and presents several advantages relative to proteinaceous fibrils. First, the chemi-fibrils form instantly when diluted from DMSO into cell culture, and the fibrillar structure is very reproducible. Cell death occurs within a few hours, making chemi-fibrils highly amenable for high-throughput screening to look for inhibitors. Lastly, high-yield chemical synthesis provides unlimited material and the potential for detailed structure-activity studies. We believe that our findings, paired with the genetic and pharmacological tools presented, will help future research to better compare the mechanisms for chemi-fibril and proteinaceous fibril–induced cell death.

Received 8 April 2014; accepted 20 August 2014;
published online 28 September 2014

METHODS

Methods and any associated references are available in the online version of the paper.

Accession codes. Cambridge Crystallographic Data Centre. Crystal structure data for 1541 are deposited under accession code CCDC 1009102.

References

1. Jucker, M. & Walker, L.C. Self-propagation of pathogenic protein aggregates in neurodegenerative diseases. *Nature* **501**, 45–51 (2013).
2. Eisenberg, D. & Jucker, M. The amyloid state of proteins in human diseases. *Cell* **148**, 1188–1203 (2012).
3. Wolan, D.W., Zorn, J.A., Gray, D.C. & Wells, J.A. Small-molecule activators of a proenzyme. *Science* **326**, 853–858 (2009).
4. Zorn, J.A., Wille, H., Wolan, D.W. & Wells, J.A. Self-assembling small molecules form nanofibrils that bind procaspase-3 to promote activation. *J. Am. Chem. Soc.* **133**, 19630–19633 (2011).
5. Zorn, J.A., Wolan, D.W., Agard, N.J. & Wells, J.A. Fibrils colocalize caspase-3 with procaspase-3 to foster maturation. *J. Biol. Chem.* **287**, 33781–33795 (2012).
6. Bassik, M.C. *et al.* Rapid creation and quantitative monitoring of high coverage shRNA libraries. *Nat. Methods* **6**, 443–445 (2009).
7. Bassik, M.C. *et al.* A systematic Mammalian genetic interaction map reveals pathways underlying ricin susceptibility. *Cell* **152**, 909–922 (2013).
8. Kampmann, M., Bassik, M.C. & Weissman, J.S. Integrated platform for genome-wide screening and construction of high-density genetic interaction maps in mammalian cells. *Proc. Natl. Acad. Sci. USA* **110**, E2317–E2326 (2013).
9. Weiss, W.A., Taylor, S.S. & Shokat, K.M. Recognizing and exploiting differences between RNAi and small-molecule inhibitors. *Nat. Chem. Biol.* **3**, 739–744 (2007).
10. Crawford, E.D. *et al.* The DegraBase: a database of proteolysis in healthy and apoptotic human cells. *Mol. Cell. Proteomics* **12**, 813–824 (2013).
11. Mahrus, S. *et al.* Global sequencing of proteolytic cleavage sites in apoptosis by specific labeling of protein N termini. *Cell* **134**, 866–876 (2008).
12. Wiita, A.P., Seaman, J.E. & Wells, J.A. Global analysis of cellular proteolysis by selective enzymatic labeling of protein N-termini. *Methods Enzymol.* **544**, 327–358 (2014).
13. Wolpaw, A.J. *et al.* Modulatory profiling identifies mechanisms of small molecule–induced cell death. *Proc. Natl. Acad. Sci. USA* **108**, E771–E780 (2011).
14. Holmes, B.B. *et al.* Heparan sulfate proteoglycans mediate internalization and propagation of specific proteopathic seeds. *Proc. Natl. Acad. Sci. USA* **110**, E3138–E3147 (2013).
15. Owen, S.C., Doak, A.K., Wassam, P., Shoichet, M.S. & Shoichet, B.K. Colloidal aggregation affects the efficacy of anticancer drugs in cell culture. *ACS Chem. Biol.* **7**, 1429–1435 (2012).
16. Owen, S.C. *et al.* Colloidal drug formulations can explain "bell-shaped" concentration-response curves. *ACS Chem. Biol.* **9**, 777–784 (2014).
17. Kampmann, M., Bassik, M.C. & Weissman, J.S. Functional genomics platform for pooled screening and generation of mammalian genetic interaction maps. *Nat. Protoc.* **9**, 1825–1847 (2014).
18. Tisdale, E.J., Bourne, J.R., Khosravi-Far, R., Der, C.J. & Balch, W.E. GTP-binding mutants of rab1 and rab2 are potent inhibitors of vesicular transport from the endoplasmic reticulum to the Golgi complex. *J. Cell Biol.* **119**, 749–761 (1992).
19. Bucci, C., Thomsen, P., Nicoziani, P., McCarthy, J. & van Deurs, B. Rab7: a key to lysosome biogenesis. *Mol. Biol. Cell* **11**, 467–480 (2000).
20. Stenmark, H., Vitale, G., Ullrich, O. & Zerial, M. Rabaptin-5 is a direct effector of the small GTPase Rab5 in endocytic membrane fusion. *Cell* **83**, 423–432 (1995).
21. Seto, S., Tsujimura, K. & Koide, Y. Rab GTPases regulating phagosome maturation are differentially recruited to mycobacterial phagosomes. *Traffic* **12**, 407–420 (2011).
22. Stenmark, H. Rab GTPases as coordinators of vesicle traffic. *Nat. Rev. Mol. Cell Biol.* **10**, 513–525 (2009).
23. Münch, C., O'Brien, J. & Bertolotti, A. Prion-like propagation of mutant superoxide dismutase-1 misfolding in neuronal cells. *Proc. Natl. Acad. Sci. USA* **108**, 3548–3553 (2011).
24. Weinstein, J.N., Yoshikami, S., Henkart, P., Blumenthal, R. & Hagins, W.A. Liposome-cell interaction: transfer and intracellular release of a trapped fluorescent marker. *Science* **195**, 489–492 (1977).
25. Shimbo, K. *et al.* Quantitative profiling of caspase-cleaved substrates reveals different drug-induced and cell-type patterns in apoptosis. *Proc. Natl. Acad. Sci. USA* **109**, 12432–12437 (2012).
26. Wiita, A.P. *et al.* Global cellular response to chemotherapy-induced apoptosis. *Elife* **2**, e01236 (2013).
27. Fraley, C. & Raftery, A.E. Model-based clustering, discriminant analysis, and density estimation. *J. Am. Stat. Assoc.* **97**, 611–631 (2002).
28. Duewell, P. *et al.* NLRP3 inflammasomes are required for atherogenesis and activated by cholesterol crystals. *Nature* **464**, 1357–1361 (2010).
29. Halle, A. *et al.* The NALP3 inflammasome is involved in the innate immune response to amyloid-β. *Nat. Immunol.* **9**, 857–865 (2008).
30. Huff, M.E., Balch, W.E. & Kelly, J.W. Pathological and functional amyloid formation orchestrated by the secretory pathway. *Curr. Opin. Struct. Biol.* **13**, 674–682 (2003).
31. Novitskaya, V., Bocharova, O.V., Bronstein, I. & Baskakov, I.V. Amyloid fibrils of mammalian prion protein are highly toxic to cultured cells and primary neurons. *J. Biol. Chem.* **281**, 13828–13836 (2006).
32. Yao, J. *et al.* Neuroprotection by cyclodextrin in cell and mouse models of Alzheimer disease. *J. Exp. Med.* **209**, 2501–2513 (2012).
33. Walsh, D.M. & Selkoe, D.J. Aβ oligomers—a decade of discovery. *J. Neurochem.* **101**, 1172–1184 (2007).

Acknowledgments

We would like to thank F. Brodsky, B. Shoichet, W. Degrado, M. Zhuang, A. Wiita, Z. Hill, J.T. Koerber, N. Thomsen, J. Watts, S.-A. Mok and J. Rettenmaier for insightful discussions and/or critical reading of the manuscript. A special thanks to Y. Chen (cell culture and laboratory practices expertise), Y. Cheng and M. Braunfield (EM), A. Doak (DLS), H. Tran (yeast expertise), D. Larsen (live cell imaging), J. Lund (deep sequencing), M. Hornsby and K. Verba (fluorescence) and T. Matsuguchi (qPCR) for technical help. This work was supported, in whole or in part, by US National Institutes of Health grant R01 CA136779 (to J.A.W.), R01 CA097061 (to B.R.S.) and F32AI095062 (to V.J.V.) and by the Howard Hughes Medical Institute (to B.R.S. and J.S.W.). J.A.Z. received an Achievement Rewards for College Scientists Foundation Award and a Schleroderma Research Foundation Evnin-Wright Fellowship. M.K. was supported by a postdoctoral fellowship from the Jane Coffin Childs Memorial Fund. O.J. is the recipient of a Banting Postdoctoral Fellowship funded by the Canadian Institutes of Health Research and the Government of Canada. O.J. and M.K. both received a fellowship from the University of California–San Francisco Program for Breakthrough Biomedical Research, which is funded in part by the Sandler Foundation.

Author contributions

O.J. performed the cell culture experiments, EM, DLS, flow cytometry and fluorescence microscopy under J.A.W.'s supervision. O.J. performed the shRNA screen and made the stable cell lines, with help and guidance from M.K. and M.C.B. and supervision of J.S.W.; M.K. analyzed the deep-sequencing data. J.A.Z. synthesized the 1541 analogs and provided general expertise on the project. A.L.R. performed the crystallography and structure determination. V.J.V. performed the liposome leakage assays. K. Shimbo and N.J.A. performed the degradomics experiments, and O.J. compiled the results. K. Shimada performed the modulatory profiling experiments under B.R.S.'s supervision. O.J. and J.A.W. wrote the manuscript with contributions from M.K., J.A.Z. and B.R.S., with input from all authors.

Competing financial interests

The authors declare no competing financial interests.

Additional information

Supplementary information is available in the online version of the paper. Reprints and permissions information is available online at http://www.nature.com/reprints/index.html. Correspondence and requests for materials should be addressed to J.A.W.

ONLINE METHODS

Chemical synthesis and reagents. Synthesis, purification and characterization of 1541 and related analogs were carried out as previously described[3]. Inhibitors were purchased as following and used as is: brefeldin A (Sigma, B5936, >98%), STS (Cayman chemicals, 81590, >98%), methyl-β-cyclodextrin (Sigma, C4555), cytochalasin D (Sigma, C2618, >98%), chloropromazine (Sigma, C8138, >98%), chloroquine (Sigma, C6628, >98%) and bafilomycin A1 (Sigma, B1793, >90%).

TEM. Chemi-fibrils were generated by diluting DMSO stocks directly into water, buffer or cell culture medium. Solutions were immediately placed on glow-discharged grids (formvar/carbon-coated 400 mesh copper grids from Ted Pella, Inc.) after mixing at room temperature. 1 µl of sample was adsorbed onto the grids for 30 s followed by wash in 25 µl water (2×) followed by negative staining in 25 µl drops (×2) of filtered 1% uranyl acetate, pH 7.4. The grids were viewed in a Tecnai T12 electron microscope (Eindhoven, the Netherlands) at 120 kV. The images were recorded on a Gatan 4k × 4k CCD camera (Gatan, Inc., Pleasanton, CA) at 52,000× magnification, unless otherwise specified.

DLS assays. Particles of 1541 were detected by DLS (Wyatt Technology DynaPro MS/X). The instrument has a 55 mW laser at 826.6 nm, and the laser power was set to 100% unless otherwise noted. The intensity of scattered light was monitored at an angle of 90°. Again, compound mixtures were prepared in standard assay buffer (50 mM HEPES, pH 7.4, 50 mM KCl, 0.1 mM EDTA, 1 mM DTT and 0.1% CHAPS) or in water. 1541 was diluted in the buffer from concentrated DMSO stocks, and water containing an equivalent amount of DMSO was used as control sample to determine the background. Mixtures were analyzed immediately. Each measurement was repeated in triplicate.

Crystallography and structure determination of 1541. Very small pale yellow needle crystals of 1541 were grown by the slow evaporation of a DMF solution at 0 °C. Diffraction data were collected using a Bruker D8 platform diffractometer equipped with a Nonius FR-591 rotating-anode Cu source and an APEXII CCD detector. The crystal packing revealed a C2/c space group, and a total of 3,076 reflections were used for the structure determination. A structural figure with probability ellipsoids is shown in **Supplementary Figure 1**.

Cell culture. K562 cells were grown in RPMI medium supplemented with glutamine, penicillin-streptomycin and 10% FBS. HeLa cells and 293T cells were grown in DMEM medium with high glucose and were further supplemented with glutamine, penicillin-streptomycin and 10% FBS. Cells were infected lentivirus-packaged plasmids expressing a puromycin resistance gene, mCherry and an shRNA in a minimal mir30a-context (plasmid backbone pMK1098 for individual shRNA experiments and plasmid backbone pMK1047 for pooled libraries[7]). For individual shRNA experiments, lentivirus was produced in six-well plates, and 1 ml viral supernatant adjusted to 8 µg/ml polybrene was used to infect 1×10^5 cells by spin infection at 1,000*g* for 2 h at 33 °C (ref. 7). For library infections, virus was produced in 15-cm plates of 293T cells. Library infections were performed on 3.5×10^7 cells in 70 ml virus supernatant with 8 µg/ml polybrene. Cells were divided into wells of a six-well plate and spin-infected as above to get a target multiplicity of infection of ~30–40%, as monitored by mCherry expression. This low multiplicity of infection was chosen such that most cells would only express one shRNA. Three days after infection, cells were selected with puromycin at 0.7 µg/ml to increase the fraction of infected cells to ~85%, washed and transferred into fresh medium, and allowed to recover for 2 d.

Primary shRNA screen. The design and generation of shRNA libraries in K562 cells was performed as previously described[7]. Two libraries covering more than 4,000 genes were used in these studies. The shRNA screen was performed in two biological replicates. For both replicates, a population size of at least ~150 million live cells was maintained at all times, of which ~85% were infected with an element of the shRNA library, as measured by mCherry fluorescence, to guarantee an average representation of at least ~1,000 cells per shRNA. K562 cells were treated with 1541 or DMSO for 24 h, after which the cell culture medium was replaced with drug-free medium to let the cells recover over 2–4 days before treating the cells for another cycle. Cell density was re-adjusted to 0.5×10^6 cells/ml daily, and cell growth was monitored using a Scepter cell counter (Millipore) (**Supplementary Fig. 7**). After more than 20 d of differential growth, 300 million cells were lysed for each the treated and untreated pools and the DNA was extracted. As previously described[7,17], DNA was size-fractionated, and the shRNA-encoding cassette was PCR-amplified using primers that introduced Illumina adaptors and four-nucleotide indices. PCR products were gel-purified and deep sequenced on an Illumina HiSeq 2500. Computational analysis was performed using GImap software (http://gimap.ucsf.edu) as previously described[8,17].

Secondary shRNA validation. shRNAs targeting individual hit genes from the primary screen were cloned into vector pMK1098 (ref. 8), in which shRNAs are expressed from an EF1A-promoter driven mRNA also encoding puromycin resistance and the fluorescent protein mCherry. Sequences corresponding to the shRNA guide strands were as follows: RAB1A_8: 5′-TTTAACATTGGACTTCTCAGCA-3′, RAB1A_10: 5′-ATGGAAAGTGACAGACACTGCT-3′, RAB2A_3: 5′-TTATACAAGAATTTGACGGATT-3′, RAB2A_4: 5′-TTATTAATGTCAAAGACTCCT-3′, ATP6V0C_2: 5′-TAAATCATCCGCATACACAGAG-3′, Negative control shRNA: 0.5′- TTTCTTACTCACCCTAAGAACT-3′.

qPCR. For qPCR, 5×10^6 cells were collected, and RNA was purified using an RNeasy kit (QIAGEN). 2 µg total of RNA was used for reverse transcription using AMV RT (Roche) and oligo dT. Samples were then quantified by qPCR using Go-Taq polymerase (Promega) and SYBR green using a LightCycler 480 (Roche).

Cell viability and caspase activity assays. Using one plate per time point, 2×10^3 to 5×10^3 cells were plated onto a 96-well plate the day before the experiment for adherent cells or on the same day for K562 or other suspension cell lines. Cell viability was monitored using CellTiter-Glo, and DEVDase activity was measured using Caspase-Glo 3/7 (Promega). Detection reagents were added at a 1:1 volume ratio directly into the wells as per manufacturer instructions, and luminescence was recorded on a SpectraMax M5 (Molecular Devices).

Flow cytometry and cellular imaging. Flow cytometry data were obtained on a FACSAria II (BD Biosciences) cytometer. The percentages of infected cells were obtained by gating live cells based on forward and side scattering for 10,000 events or more, and mCherry levels were then measured. Live cell imaging was performed on a Nikon Ti-E Microscope wide-field epifluorescence system equipped with a 37 °C incubation chamber and CO_2 control or a Zeiss Observer Z1 for shorter experiments. Colocalization experiments with LysoTracker were performed on a Nikon Ti-E Microscope spinning disk confocal. Images were taken using oil immersion lens with maximum magnification of 63× or 100× in 35-mm no. 1.5 coverslip bottom dishes (MatTek Corporation). Excitation and emission wavelengths of 405 nm and 460 nm, respectively, were used to monitor 1541. The organelle markers were all purchased from Invitrogen: Hoechst 33342 (H-3570), ER-Tracker Red (E34250) LysoTracker Red (L-7528), MitoTracker Green (M7514). Image processing and analysis was done using ImageJ or Fiji.

Liposomes. Lipid thin films containing 60% DPPC and 40% cholesterol were prepared in 10 × 25 mm glass test tubes by rotary evaporation under reduced pressure followed by high vacuum for 18 h. The resultant lipid film was rehydrated in 500 µl of 20 mM HEPES, 20 mM MES buffer containing 100 mM carboxyfluorescein at pH 7.4 (5 mM final concentration). The formulation was then heated to 55 °C for 1 h and sonicated at 55 °C for 15 min and extruded through 100-nm polycarbonate membranes to achieve a homogeneous distribution of particles of 100 nm in diameter, as determined by Malvern Zetasizer NanoZS. Liposomes were then eluted through Sephadex G-25 resin to remove unencapsulated carboxyfluorescein using an isotonic buffer of 20 mM HEPES, 20 mM MES and 100 mM NaCl. Leakage experiments were performed by monitoring the increase in carboxyfluorescein fluorescence (excitation: 490 nm; emission: 535 nm). Solutions of 1541 were prepared in DMSO, and 5 µl of each solution was added directly to the liposomes. Fluorescence was monitored for 5 min, and 10 µl of a 1% solution of Triton X-100 was added to lyse the liposomes to determine the total carboxyfluorescein present in the sample. Percent leakage was calculated by normalizing the increase in fluorescence over time to the total fluorescence of the sample. For TEM image acquisition, chemi-fibrils (25 µM of 1541) were prepared in water, liposomes were added to the fibrils and 1 µl of the mixed solution was placed on a grid as quickly as possible. Staining and data acquisition were performed as described above.

N-terminomics and MS. Free N termini in cells either treated or not treated with 1541 were detected as previously described[12]. Two independent cellular experiments were carried out. First, HeLa S3 (3×10^9 cells) were grown in the presence or absence of EGF (100 ng/ml for 10 min) and treated with 25 μM of 1541 fibrils for 16 h. Cell lysates were collected, free N termini were biotinylated and captured, and on-bead trypsin-digested protein fragments were identified by LC/MS/MS on a QSTAR Elite (AB Sciex). In the second experiment, B lymphoblast (DB) cells were treated with 12.5 μM of 1541B fibrils for 5 h, 7 h, 9 h, 10.5 h, 12 h, 16 h and 17.5 h, all in separate dishes containing more than 4×10^8 cells. Samples were processed as described above. Peptide identification was performed using Protein Prospector (v. 5.6 or higher; University of California–San Francisco), and all data sets were combined herein. All spectra were searched using the full human SwissProt database (downloaded 15 December 2009 or 8 July 2011) with reverse sequence database for false discovery rate determination. Search parameters included fixed modifications (N-terminal aminobutyric acid and cysteine carbamidomethylation), variable modifications (methionine-loss (N terminus) and methionine oxidation), up to three missed tryptic cleavages, C-terminal trypsin cleavage, nonspecific cleavage at the N terminus, parent mass tolerance of 100 p.p.m. and a fragment mass tolerance of 200 p.p.m. The expectation value cut-off was adjusted to maintain a <1% false-discovery rate at the peptide level in each sample.

Modulatory profiling. Chemi-fibrils were examined using modulatory profiling, following the method described previously with a slight modification[13]. In brief, fibrosarcoma HT-1080 and engineered BJeLR tumor cells were treated with the three compounds in a 14-point, two-fold dilution series. The highest concentrations used were 1541 (30.4 μM) or the hydroxyl analog 1541B (31.5 μM). The cells were simultaneously treated with a set of cell death modulators[13] to produce modulatory profiles. The experiment was done in biological duplicates. The resulting modulators' effects on the lethality of 1541 and its analog, alongside lethal compounds with known mechanism of action, were assessed by computing the difference between area under dose-response curves with or without each modulator treatment. Assembled profiles were analyzed with model-based clustering and visualized in a heat map. A modulatability score was computed by averaging the absolute values of all the modulators' effects. Computation and visualization were performed using the R statistical language except for that in **Figure 3c**. The dose-response curve was generated with GraphPad Prism 5. The significance of difference between EC_{50} values for two dose-response curves was computed with extra sum-of-squares F test. For the z-VAD-fmk experiment (**Fig. 5c**), HT-1080 fibrosarcoma or BJeLR engineered fibroblasts were seeded into 384 well plates at 1,000 cells/well. They were pretreated with 20.9 μg/ml (45 μM) of zVAD-fmk for 1 h before addition of lethal compounds. Cells were incubated for 48 h. zVAD-fmk was purchased from ENZO (BIOMOL).

doi:10.1038/nchembio.1639